JACS
JOURNAL OF THE AMERICAN CHEMICAL SOCIETY
pubs.acs.org/JACS
Article

Emergence of Electric Fields at the Water–C12E6 Surfactant Interface

Rahul Gera, Huib J. Bakker,* Ricardo Franklin-Mergarejo, Uriel N. Morzan, Gabriele Falciani, Luca Bergamasco, Jan Versluis, Indraneel Sen, Silvia Dante, Eliodoro Chiavazzo, and Ali A. Hassanali*

Cite This: https://doi.org/10.1021/jacs.1c05112

ABSTRACT: We study the properties of the interface of water and the surfactant hexaethylene glycol monododecyl ether (C12E6) with a combination of heterodyne-detected vibrational sum frequency generation (HD-VSFG), Kelvin-probe measurements, and molecular dynamics (MD) simulations. We observe that the addition of the hydrogen-bonding surfactant C12E6, close to the critical micelle concentration (CMC), induces a drastic enhancement in the hydrogen bond strength of the water molecules close to the interface, as well as a flip in their net orientation. The mutual orientation of the water and C12E6 molecules leads to the emergence of a broad (∼3 nm) interface with a large electric field of ∼1 V/nm, as evidenced by the Kelvin-probe measurements and MD simulations. Our findings may open the door for the design of novel electric-field-tuned catalytic and light-harvesting systems anchored at the water–surfactant–air interface.

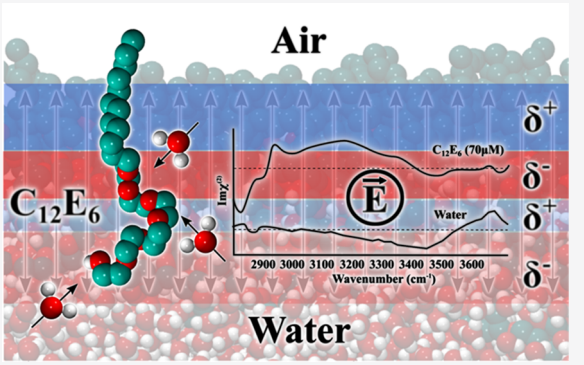

INTRODUCTION

Over the last few decades, there has been a significant interest in the behavior of water at inorganic and biological interfaces.[1] Although it is well appreciated that the structure, dynamics, and electronic properties of water change near interfaces, many aspects regarding the spatial extent and magnitude of these perturbations continue to be a topic of intense theoretical and experimental study.[2] One aspect of specific interest that has recently emerged is the appearance of electric fields near interfaces and their effect on chemical reactivity.[3]

Electric-field fluctuations are at the heart of chemical reactions such as electron and proton transfer in aqueous solution, in the active sites of proteins, or near DNA.[4] The role of the electric fields is particularly pertinent when there is a breaking of symmetry in the system: for example, at aqueous interfaces due to the presence of ionic charges leading to the formation of a double layer.[5] Even in the absence of ionic charges, it has been noted that an electric field can be created by a network of oriented water molecules at interfaces.[6] However, the precise microscopic origin of such electric fields in heterogeneous environments involving water and other solutes remains elusive, since different species can contribute in nontrivial ways to alter the electrical potentials. The ability to control these electric fields has enormous potential for the development of green-energy technologies.[3b,f,7]

In this study we investigate the surface of an aqueous solution of the surfactant hexaethylene glycol monododecyl ether (C12E6), using a combination of heterodyne-detected vibrational sum frequency generation (HD-VSFG), Kelvin-probe vibrating electrode measurements, and molecular dynamics (MD) simulations. C12E6 forms one of the members of a well-studied class of nonionic surfactants that contain a poly(ethylene oxide) group as the polar headgroup and an aliphatic chain as the tail. This class of surfactants has been extensively studied over the years for their physical properties.[8] Moreover, C12E6 is an interesting system, as this molecule shows a high potential in the formation of soap films for artificial photosynthesis applications.[8h]

Our findings indicate that C12E6 creates a broad (∼3 nm) interface with strongly enhanced dynamic correlations and a hydrogen-bonding network involving both copenetrated water and surfactant groups. The surfactant also induces changes in the water orientation at the interface. These structural changes, observed both by HD-VSFG measurements and MD simulations, create a net interfacial electric field of ∼1 V/nm pointing toward the bulk, which is confirmed by Kelvin-probe surface potential experiments.

Received: May 18, 2021

MATERIALS AND METHODS

Experiments. *Heterodyne-Detected Surface Sum-Frequency Generation (HD-VSFG).* Surface-sensitive VSFG has matured over the years in providing a molecular-level description of interfaces. This technique has been discussed in detail in different reports.[1a,c,f,9] In brief, we perform VSFG by focusing two laser pulses with frequencies ω_{IR} and ω_{vis}, on the surface with spatial and temporal overlap. The mid-infrared pulse (ω_{IR}) is resonant with the vibrational frequencies of molecules present at the interface, while and ω_{vis} is a visible pulse used for upconverting the signal to the sum frequency ω_{SFG} ($\omega_{SFG} = \omega_{IR} + \omega_{vis}$). Light at ω_{SFG} can only be created in noncentrosymmetric media under an electric dipole approximation, thus making the sum-frequency generation process highly surface specific. The intensity of the sum frequency light created is given by $I_{SFG} \propto |\chi^{(2)}|^2 I_{vis} I_{IR} L_{SFG}^2 L_{IR}^2 L_{vis}^2$, where $\chi^{(2)}$ is the macroscopic second-order nonlinear susceptibility, I_{vis} and I_{IR} are the intensities of the incoming visible and mid-infrared radiation, respectively, and L_{SFG}, L_{IR}, L_{vis} are the Fresnel coefficients for the SFG, IR, and visible light, respectively. We also measure the VSFG spectrum of a reference sample for which the sum-frequency generation is nonresonant, to normalize the measured signal on the spectral intensity distribution of the infrared pulse. $\chi_{ref}^{(2)}$ is independent of ω_{IR} and ω_{vis}. Thus, using

$$\frac{I_{SFG}(\omega_{SFG})}{I_{ref}(\omega_{SFG})} = \frac{|\chi^{(2)}(\omega_{SFG} = \omega_{IR} + \omega_{vis})|^2}{|\chi_{ref}^{(2)}(\omega_{SFG} = \omega_{IR} + \omega_{vis})|^2}$$

a frequency-dependent $|\chi^{(2)}(\omega_{SFG} = \omega_{IR} + \omega_{vis})|^2$ or the VSFG spectrum is obtained. $\chi^{(2)}(\omega_{SFG} = \omega_{IR} + \omega_{vis})$ can often be expressed as a sum of Lorentzian vibrational resonances and a nonresonant background signal

$$\chi^{(2)}(\omega_{SFG} = \omega_{IR} + \omega_{vis}) = A_{NR} + \sum_n \frac{A_n}{\omega_n - \omega_{IR} - i\Gamma_n}$$

where ω_n, A_n, and Γ_n are the frequency, amplitude, and damping constant of the vibrational mode n of the molecule at the interface, respectively, and A_{NR} is the nonresonant background. A direct determination of $\chi^{(2)}(\omega_{SFG})$ from the conventional intensity VSFG is not possible, as the intensity VSFG is proportional to $|\chi^{(2)}|^2$, which strongly depends on the interference of the nonresonant background and the resonant contributions to $\chi^{(2)}$. This problem can be solved by performing heterodyne-detected VSFG (HD-VSFG),[1a,9a,10] which gives direct access to the real and imaginary parts of $\chi^{(2)}$. $\mathrm{Im}\chi^{(2)}$ is a direct representation of the vibrational spectrum of the molecules at the interface and can thus be directly compared to bulk infrared and Raman measurements.[1a,9a,10] Moreover, the sign of $\mathrm{Im}\chi^{(2)}$ reflects the orientation of the molecular group that carries the normal vibrational mode.

The details of the experimental setup have been previously reported.[11] Briefly, the ~3 mJ, 35 fs, 800 nm pulses from a regenerative Ti:sapphire amplifier (Coherent Legend), working at a 1 kHz repetition rate, are split into two parts. About 2 mJ of the fundamental beam is used to generate a mid-infrared (mid-IR) beam using a tunable home-built optical parametric amplifier (OPA) and a difference-frequency-generation (DFG) stage. The ω_{IR} value from the OPA + DFG was centered at ~3000 nm, and the pulses had an energy of ~12−14 μJ. Another part of the fundamental beam is sent through an etalon to stretch the femtosecond beam to a few picoseconds and to narrow the frequency bandwidth to 15 cm^{-1}. This beam acts as ω_{vis}. In HD-VSFG we generate ω_{SFG} both from a gold substrate that acts as a local oscillator (LO) and from the sample. The two SFG responses are delayed in time with respect to each other by passing the local oscillator ω_{SFG} beam through a silica plate (~1 mm). The two ω_{SFG} beams are sent into a monochromator and detected with an electron-multiplied charge-coupled device (EMCCD, Andor Technologies). The interference pattern of the two beams makes it possible to extract the real and imaginary parts of $\chi^{(2)}$ using a Fourier transformation. $\mathrm{Im}\chi^{(2)}$ is obtained by comparing the HD-VSFG signal with a reference HD-VSFG signal whose phase of the SFG light is known.[1a,12] We obtain the reference HD-VSFG signal from a z-cut quartz crystal. The typical acquisition time of an HD-VSFG spectrum is 55 s. The measurements reported in this paper are recorded with a ssp (ω_{SFG}, ω_{vis}, ω_{IR}) polarization combination.

The stock of C12E6 surfactant (≥99% pure) was purchased from Anatrace and used without further purification. We prepared solutions with different surfactant concentrations in Millipore water.

Kelvin-Probe Surface Potential. The Kelvin-probe experiments were carried out using a custom-made reduced volume (50 mm × 148 mm) Teflon Langmuir trough (KSV-NIMA, Finland). The trough was placed under a hood and equipped with a surface potential sensor with a vibrating electrode (SPOT, KSV-NIMA). The surface pressure was measured in the same trough using a Pt-Wilhelmy probe. The experimental setup is shown in the Figure S4 in the Supporting Information.

Before use, the Teflon trough was carefully cleaned with ethanol and rinsed several times with ultrapure water to remove any trace of contaminants. The SPOT stainless-steel counter electrode was treated in a UV/ozone chamber for 15 min before placing it in the trough. The trough was filled with a measured volume of ultrapure water (43 mL), and the water surface was carefully cleaned by a vacuum aspirator. The measurements were carried out at 22 °C.

The surface pressure of the pure water was given a reference value of 0 mN/m. The vibrating electrode was placed at 2 mm above the surface of the pure water, and a baseline recording was started. After 300 s, a small volume of the surfactant stock solution (0.04 M) was accurately measured and injected at the bottom of the trough using a Hamilton syringe to reach the desired final concentration (c = 0.07 mM). At the same time, a corresponding volume of water was removed from the trough, in order to minimize the change of the water level. The surface potential changes and the surface pressure were continuously recorded for at least 6000 s (see Figure S3).

The C12E6 surfactant (BioXtra ≥98.0% (TLC), Sigma-Aldrich) was used without further purification. The surfactant was dissolved in ultrapure water (resistivity 18.2 MΩcm) at a concentration c = 0.04 M and allowed to stabilize for at least 24 h.

Computational Methods. *Molecular Dynamics Simulations.* To study the physical properties of the water−C12E6 mixture in comparison to those of the water−air interface, we performed molecular dynamics (MD) simulations of both systems. Figure 1 depicts the simulated water−C12E6 mixture. The system consists of two interfaces each composed of 48 surfactant molecules close to the critical micelle concentration (CMC).[8e,13] The cell dimensions of the periodic system are 5 nm in both the x and y directions and 30 nm in the z direction. A total of 4055 water molecules were added to build the surfactant−water system illustrated in Figure 1. More details of the simulation can be found in ref 8h.

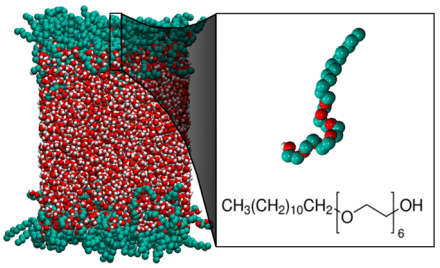

Figure 1. Representative snapshot of the simulated system. The C12E6 molecules form layers at the interfaces between water and vacuum. Carbon, oxygen and hydrogen atoms are depicted in green, red, and white, respectively.

All of the MD simulations were performed using the open source package GROMACS.[14] In these simulations, we employed the SPC model for water molecules[15] and a combination of united-atom TRaPPE and OPLS-AA[16] force fields for C12E6. The alkyl groups in C12E6 were described with a united-atom approach, whereas the oxygen atoms and OH groups were modeled explicitly. This combination of interaction potentials was adapted from previous

https://doi.org/10.1021/jacs.1c05112
J. Am. Chem. Soc. XXXX, XXX, XXX−XXX

studies[8k,17] that have been shown to reproduce several experimental parameters such as the surface tension and the thickness of the interface.[8f,18] Furthermore, we will show below that this force field provides good agreement with both the Kelvin probe and with the SFG measurements for the water−C12E6 mixture. For the short-range nonbonded interactions, a cutoff length of 1.0 nm was chosen for a shifted Lennard−Jones potential, while the long-range electrostatic interactions were taken into account via the particle mesh Ewald-switch[19] (PME-switch) method with a Coulomb switching cutoff of 1.0 nm. A long-range dispersion correction was used to truncate the van der Waals interactions. All bonds were constrained using the LINCS algorithm.[20] A time step of 2 fs was used for the Verlet integrator. All simulations were conducted in a canonical ensemble (NVT) at 298.15 K using the Nose−Hoover thermostat[21] with a time constant of 2.0 ps. The simulations were carried out for 180 ns, where the first 20 ns was used for equilibration.

Hydrogen Bond Analysis. In order to understand how the surfactant changes the water structure, we determined the topology of the hydrogen-bond network. The local water topology is defined by the distribution of the number of hydrogen bonds that are donated (D) and accepted (A) by a water molecule.[22] Far away from the interface, water molecules will only participate in hydrogen bonds with other water molecules, whereas close to the interface they can form hydrogen bonds both with other water molecules and with surfactant headgroups. The hydrogen bonds were defined using the criterion developed by Luzar and Chandler.[23]

Information Theory Metrics to Study Collective Water−Surfactant Dynamics. We quantified the correlated motions of water and surfactant molecules with a degree centrality metric (Dc).[24] The Dc is a score, assigned to every atom in the system, that in this study accounts for the total dynamic correlation between that atom and its neighborhood.

In order to obtain a Dc metric, we utilized the linear approximation of the mutual information (MI) introduced by Lange et al.[25] The mutual information between two particles is defined as

$$\mathrm{MI}[x_i, x_j] = H[x_i] + H[x_j] - H[x_i, x_j] \tag{1}$$

where x_i represents the positional fluctuations ($x_i = \langle x_i - x_i \rangle$, x_i being the three-dimensional position vector) and H denotes the entropy of the random variables. The positivity of $\mathrm{MI}[x_i,x_j]$ rests on the inequality $H[x_i,x_j] \leq H[x_i] + H[x_j]$, which becomes an equality if both variables are independent.

The linear mutual information (LMI) relies on a Gaussian approximation of the probability density that can be expressed as

$$p(x_i, x_j) = \frac{1}{8\pi^3 \det(Cov_{ij})}\left(-\frac{1}{2}(x_i, x_j)\mathrm{Cov}_{ij}^{-1}(x_i, x_j)^T\right) \tag{2}$$

where $\mathrm{Cov}_{ij} = \langle (x_i, x_j)^T (x_i, x_j) \rangle$ is the covariance matrix, and the entropies H are evaluated analytically as

$$H(x_i, x_j) = \frac{1}{2}[q + \ln \det \mathrm{Cov}_{ij}] \tag{3}$$

where $q = 6(1 + \ln 2\pi) = 17.02726$. In this study we focus on the correlations that arise from local directional interactions (i.e., hydrogen bond, dipole−dipole, or van der Waals interactions). Hence, our estimator accounts for the correlation between each atom and its most immediate neighbors. Therefore, instead of the standard covariance we defined a local covariance $\widetilde{\mathrm{Cov}_{ij}}$ as

$$(\widetilde{\mathrm{Cov}_{ij}}) = (x_i, x_j)^T (x_i, x_j) \exp -[(x_i - x_j)/\lambda]^2 \tag{4}$$

The exponential term in eq 4 damps the covariance contribution associated with distant atoms and leaves only the local components with a characteristic distance parameter of λ. In the present work we employed $\lambda = 5$ Å, which accounts for the first and second solvation shells.

We can now define a local linear mutual information (LLMI) as

$$\mathrm{LLMI}_{ij} = \frac{1}{2}(\ln \det \widetilde{\mathrm{Cov}_i}) + (\ln \det \widetilde{\mathrm{Cov}_j}) - (\ln \det \widetilde{\mathrm{Cov}_{ij}}) \tag{5}$$

where $\widetilde{\mathrm{Cov}_i} = \langle (x_i)^T (x_i) \rangle$ represents the marginal covariance. With this definition we can introduce our D_c metric as the total LLMI per neighbor:

$$D_c^i = \sum_j^N \frac{\mathrm{LLMI}_{ij}}{\langle \exp -[(x_i - x_j)/\lambda]^2 \rangle} \tag{6}$$

where D_c^i is the degree centrality for the ith atom in the system, indicating the strength of the dynamic "cross-talk" between atom i and its neighbors.

The D_c distribution can be projected on the perpendicular axis to the surfactant plane (z axis), which enables a determination of the water−surfactant and water−water correlations as a function of the distance to the interface.

In an infinite time limit the D_c distribution becomes uniform due to water diffusion. Therefore, in order to retain the local properties of D_c, we extracted 20 replicas of 3 ps trajectories with a 1 fs time step. The resulting z-projected distribution is obtained by averaging the 20 replicas.

RESULTS AND DISCUSSION

We performed SFG measurements for neat water and solutions with different concentrations of C12E6 in water (see Figure 2

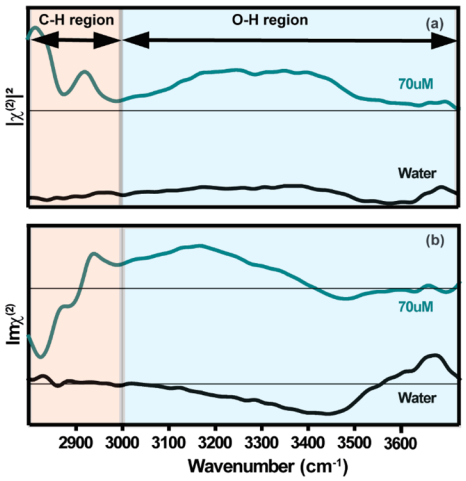

Figure 2. (a) Steady-state SFG intensity spectra of the air−C12E6−water interface measured at CMC ≈ 70 μM of C12E6. (b) Steady-state $\mathrm{Im}\chi^{(2)}$ spectra of the air/C12E6/water interface measured at CMC ≈ 70 μM of C12E6.

and Figures S1 and S2 in the Supporting Information for $|\chi^{(2)}|^2$, $\mathrm{Im}\chi^{(2)}$, and $\mathrm{Re}\chi^{(2)}$ spectra for different concentrations of C12E6). The spectrum of the neat air−water interface shown in Figure 2 consists of a broad band centered at ∼3400 cm^{-1}, attributed to the OH stretching vibrations of water molecules that donate hydrogen bonds to other water molecules, and a narrower band around 3700 cm^{-1}, assigned to the stretching vibrations of non-hydrogen-bonded water O−H groups.[9a,12a] The orientation of the water molecules at the interface can be directly obtained from the sign of $\mathrm{Im}\chi^{(2)}$. The $\mathrm{Im}\chi^{(2)}$ value of the broad band centered at ∼3400 cm^{-1} has a negative sign, whereas the $\mathrm{Im}\chi^{(2)}$ value of the narrower band around 3700 cm^{-1} is positive. This implies that the water molecules which donate hydrogen bonds to other water molecules have a net orientation of their O−H groups toward the bulk of the liquid, whereas the non-hydrogen-bond-donating hydrogens of the OH groups are directed toward the air.[9a,12a]

Adding C12E6 to water at concentrations larger than 1 μM leads to the disappearance of the band at ∼3700 cm^{-1}. This

https://doi.org/10.1021/jacs.1c05112
J. Am. Chem. Soc. XXXX, XXX, XXX−XXX

concentration is much lower than the critical micelle concentration (CMC) of C12E6, which is ∼70−80 μM.[26] (see Figure 2 and Figure S1 in the Supporting Information for a detailed comparison of the spectral evolution at different concentrations). The loss of the signal at 3700 cm^{-1} with an increasing concentration of C12E6 shows that the surface of water becomes covered by a layer of surfactant molecules. The most striking observation upon adding C12E6 is the change in sign of the $Im\chi^{(2)}$ value of the hydrogen-bonded OH groups. The negative $Im\chi^{(2)}$ value between ∼3200 and ∼3600 cm^{-1} of neat water changes to a strong positive $Im\chi^{(2)}$ value between ∼3000 and ∼3400 cm^{-1}. This change of sign for $Im\chi^{(2)}$ shows that the net orientation of the hydrogen-bonded water molecules at the surface changes from pointing toward the bulk to a net direction toward the surfactants or the air. Adding the surfactant to the solution also leads to a significant red shift of the response of the hydrogen-bonded OH groups. More specifically, the broad negative feature at ∼3400 cm^{-1} is red-shifted to a more intense positive band centered at ∼3200 cm^{-1}. The red shift of the response implies that the hydrogen bonds of the water molecules near the interface have become stronger, indicating that the water molecules form strong hydrogen bonds with the headgroups of the surfactants. It is important to note that the red shift in the spectra does not arise from hydrogen bonds being accepted by water molecules from the hydroxyl alcohol group. This hydrogen bond is not expected to be much stronger than the hydrogen bond donated by a water molecule. Instead, the red shift is explained by the strong hydrogen bonds that are donated by water molecules to the oxygen atoms of the surfactant headgroup. These oxygen atoms have a relatively large partial negative charge, thereby leading to a stronger donated hydrogen bond in comparison to that involving the top layer of water molecules to water molecules underneath.

In addition to the strong positive band at ∼3200 cm^{-1}, the $Im\chi^{(2)}$ spectrum of the C12E6 solutions also shows a weak negative feature at ∼3500 cm^{-1}. In a previous intensity SFG study by Tyrode and co-workers for solutions of C12E4, C12E5, and C12E8, which are structural analogues of C12E6, the increase of a weak response near 3500 cm^{-1} was also observed. This response was assigned to weakly hydrogen bonded water molecules in the tail region of the surfactant molecules.[8g,27] In the same work, the net orientation of the OH groups of these water molecules was studied by VSFG intensity spectra measured under different polarization conditions, using information about the hyperpolarizability tensor elements for water based on molecular symmetry.[8g,27] On the basis of this analysis, the authors concluded that the OH groups of the water molecules with vibrational frequencies of ∼3500 cm^{-1} would be oriented toward the tail of the surfactant molecules: i.e., away from bulk water. In the present HD-VSFG measurements, we determine the orientation directly from the sign of $Im\chi^{(2)}$. We observe that $Im\chi^{(2)}$ has a negative sign at these frequencies, which unambiguously shows that the weakly hydrogen bonded OH groups of water molecules between the tails of the surfactant molecules have a net orientation toward the headgroup of the surfactant or the bulk of the solution.

The addition of C12E6 also leads to an increase in signal contributions between ∼2800 and ∼3000 cm^{-1}. These signals are attributed to the CH stretching vibrations of methylene, $-CH_2-$,and methyl groups, $-CH_3$ of the ethylene oxide headgroup, and the alkyl tail group of the surfactant. The $Im\chi^{(2)}$ spectrum of C12E6 (Figure 2b) shows a negative peak at ∼2826 cm^{-1} and a negative shoulder at ∼2895 cm^{-1}, which are attributed to the symmetric stretching and the Fermi resonance of the terminal CH_3 group, respectively. In addition, a small positive band is observed at 2935 cm^{-1}, which is attributed to the asymmetric C−H stretching mode of the $-CH_3$ group. The signs of these responses show that the terminal methyl groups of the aliphatic chains of C12E6 are pointing toward the air.[8a−g] When the concentration of C12E6 is increased and approaches the CMC, the response of the C−H stretching vibrations of the surfactant molecules in the frequency region 2800−3000 cm^{-1} increases in comparison to that of the water O−H stretching vibrations (see Figure S1 in the Supporting Information). This change is a direct consequence of the evolution in the packing of the surfactant at the interface as its concentration is increased: the surface area per molecule at full surface coverage (near the CMC) corresponds to approximately ∼62 $Å^2$ per surfactant molecule.[8a] Such tight packing at the interface with increasing concentration increases the relative amplitude of the C−H stretching region in comparison to the O−H stretching region of the spectrum, in line with previously reported work with the structurally similar surfactant C12E5.[8g,27] The tighter packing with increasing surfactant concentration also leads to a narrowing of the negative $Im\chi^{(2)}$ signal at ∼3500 cm^{-1}, as can be seen in Figure S1 in the Supporting Information. This narrowing is primarily the result of a loss of signal at frequencies >3550 cm^{-1}. The initial broad signal near ∼3500 cm^{-1} reflects structural heterogeneity: i.e., a large variation in hydrogen-bond strength of the water molecules that percolate in the hydrophobic tails. As the concentration of the surfactant is increased, the alkyl tails become more closely packed, which will push part of the water molecules into the bulk and force the remaining water molecules to adopt only a few specific hydrogen-bond configurations, thereby narrowing the feature at ∼3500 cm^{-1}.

To better understand how the mutual polarization of the water and surfactant alters the dielectric properties, we measured the surface potential of the water−C12E6 interface via a vibrating-electrode method, or Kelvin probe, according to the working principle described in the Figure S4 in the Supporting Information. The potential difference is measured between an upper electrode, vibrating vertically at 2 mm above the gas−liquid interface, and a fixed counter electrode immersed in the liquid. This technique then allows a characterization of the changes in the electric potential of the air−water interface induced by surfactant monolayers. The surface potential is defined as

$$V_{surf} = V - V_0 \tag{7}$$

where V and V_0 are the potentials in the presence or absence of the surfactant monolayer, respectively.[28] Close to the CMC conditions, we find that the surface potential is +0.7 V. The positive sign in the surface potential obtained with the Kelvin-probe measurements is consistent with previous measurements of nonionic surfactants.[29]

In order to elucidate the microscopic origin of the spectral features observed in the HD-VSFG experiments and the change in the surface potential observed in the Kelvin-probe measurements, we performed molecular dynamics simulations. At the interface, water molecules can form hydrogen bonds with other water molecules as well as surfactant molecules. In particular, the hydrophilic parts of the surfactant have ether

https://doi.org/10.1021/jacs.1c05112
J. Am. Chem. Soc. XXXX, XXX, XXX−XXX

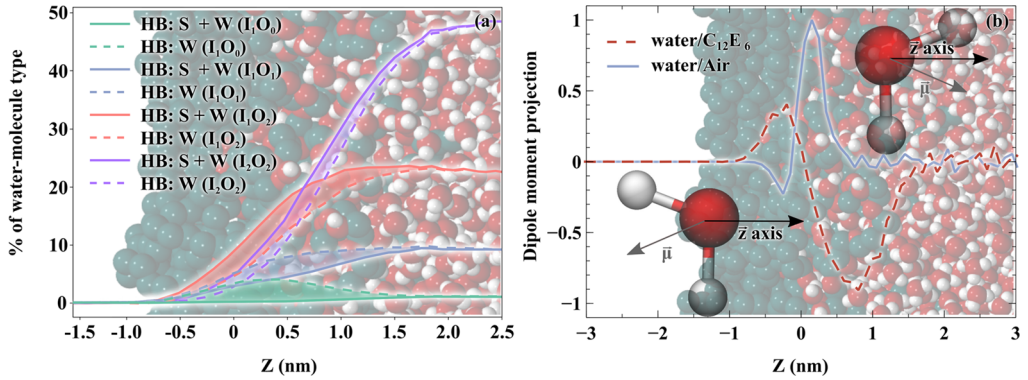

Figure 3. (a) Density of the different types of hydrogen-bonded water molecules by including surfactant groups as possible acceptors/donors of hydrogen bonds. The acronym I_xO_y refers to a water molecule with x hydrogen-bond donors and y hydrogen-bond acceptors. (b) Projection of the total dipole moment of the water molecules on the z axis as a function of the distance z from the GDI. The blue curve corresponds to the water at the air−water interface and the red dashed curve to the water at the C12E6−water interface. A positive sign indicates a net dipole orientation toward the air.

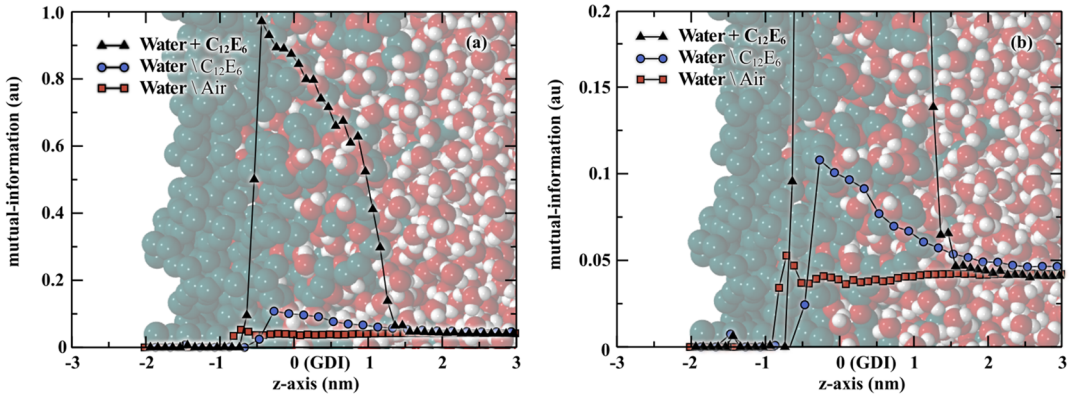

Figure 4. (a) Total z projection of the D_c distribution for the water−$C_{12}E_6$ system (black triangles), for the waters in the presence of $C_{12}E_6$ (blue circles), and for the waters in a water−air interface (red squares). (b) Amplification of the right panel. The background depicts the water−surfactant interface. Oxygen, hydrogen, and carbon atoms are depicted in red, white, and green, respectively.

oxygens (see Figure 1) that can accept hydrogen bonds from water molecules. We thus examined the concentration of some of the hydrogen-bonding patterns of water molecules, as shown in Figure 3a. The 0 on the z axis corresponds to the Gibbs dividing interface (GDI): i.e., the position along the interface where the density of water is half that of the bulk. The labels in the figure correspond to different types of water molecules. For example, I_2O_2 corresponds to water molecules that accept and donate two hydrogen bonds. The S and W labels correspond to hydrogen-bonding patterns determined either with only water molecules or with both water (W) and surfactant (S).

Interestingly, we observe that the surfactant headgroups act as hydrogen-bond acceptors, increasing the local concentration of I_2O_2 and I_1O_2 (Figure 3a). This corresponds to a decrease in non-hydrogen-bonded (dangling) O−Hs, since these water molecules now donate hydrogen bonds to the ether oxygens of the surfactant. The relative enhancement in the interfacial population of water molecules that donate and accept two hydrogen bonds points to an overall strengthening of the hydrogen-bond network, in agreement with the red shift observed in the SFG spectra (Figure 2). Interestingly, previous studies of the air−water interface have shown that there is a very thin layer of less than 0.5 nm that exhibits hydrogen-bonding structures different from those in the bulk.[1a,9a,30] In contrast, at the air−surfactant−water interface, the changes occur over a rather large length scale of approximately 3 nm.

In Figure 3b it is seen that the water molecules just below the surface acquire a strong orientation with their OH groups pointing toward the surface, in excellent agreement with the observation of a strong positive $\mathrm{Im}\chi^{(2)}$ value centered at 3200 cm^{-1} in Figure 2b. The water molecules that are in the hydrophobic region of the surfactant tails have a net orientation toward the bulk, which is again fully consistent with the observation of a negative $\mathrm{Im}\chi^{(2)}$ value near 3500 cm^{-1} in Figure 2b.

To better understand the collective dynamic perturbation of the hydrogen-bond network induced by the presence of C12E6, we turn next to employing an information theory metric. The dynamic behavior of the water molecules is significantly altered in the interfacial region. We demonstrated this by employing a degree centrality indicator (D_c) as introduced in Materials and Methods. The D_c^i value is a score associated with the degree of correlation between the motion of the ith molecule and its local environment. The more synchronized these motions are, the higher the D_c^i value becomes. In this analysis, two types of D_c distributions were employed: (i) considering only water motions ($D_{c\text{-wat}}$) and (ii) including both waters and surfactant molecules ($D_{c\text{-tot}}$).

Figure 4a shows that the $D_{c\text{-wat}}$ values increase considerably at the interface with respect to the bulk. This indicates that the intrinsic water−water correlations are enhanced at the water−surfactant interface, which is consistent with the strengthening

https://doi.org/10.1021/jacs.1c05112
J. Am. Chem. Soc. XXXX, XXX, XXX−XXX

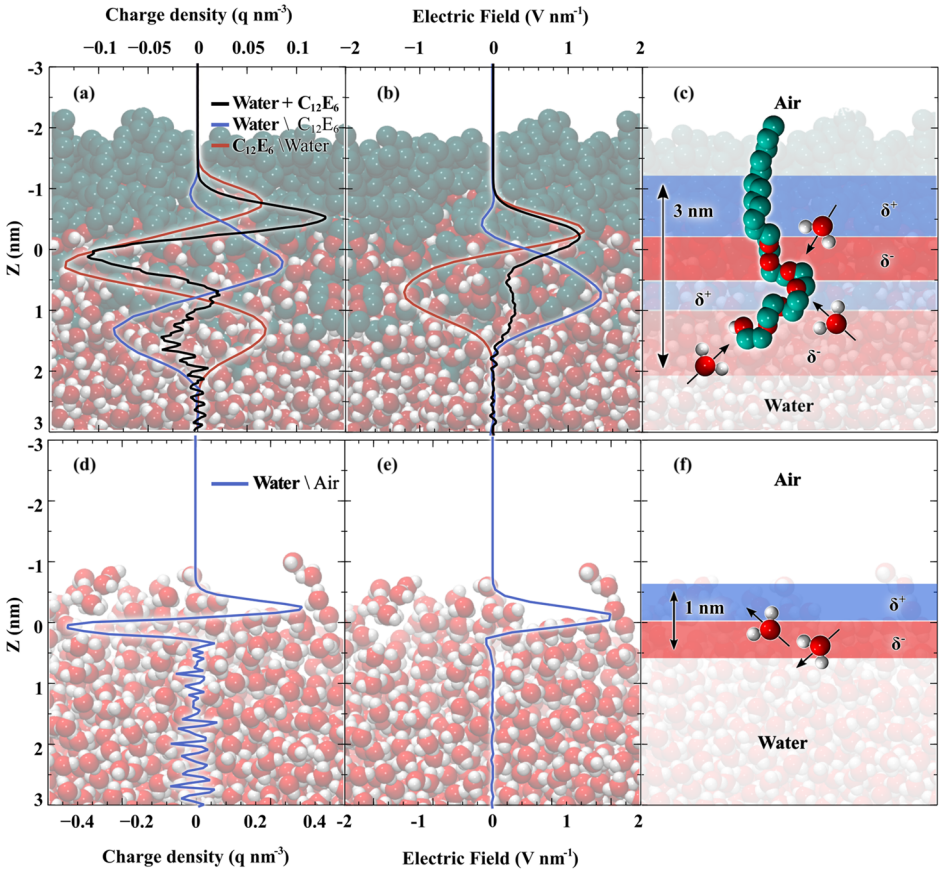

Figure 5. The top panels show the charge density (a) and electric fields (b) obtained for the surfactant−water interface. Black curves refer to the total charge density/fields, while the blue and red curves are the individual contributions coming from the water and surfactant, respectively. The bottom panels correspond to the charge density (d) and electric field (e) arising at the air−water interface. Panels (c) and (f) illustrate the molecular arrangement responsible for the ensuing charge and electric field distributions.

of the hydrogen-bond network discussed earlier. Furthermore, the interfacial increase of the $D_{c\text{-}tot}$ distribution is much more pronounced than that of the $D_{c\text{-}wat}$ values (as seen in the enlarged plot in Figure 4b). This means that the dynamic correlations between water and headgroups are much stronger than those observed between water molecules. These results demonstrate that the strong water−surfactant interactions alter the intrinsic dynamics of water molecules at the interface. The interaction with the headgroups thus amplifies the water−water correlated motions. As will be discussed below, this mutual arrangement of water and surfactant leads to considerable changes in the dielectric properties of the interface.

To understand the microscopic origins of these changes, we examined various dielectric-related properties from atomistic simulations. Figure 5a shows the total charge density profile at the water−C12E6 surfactant interface (solid black line) as well as the separate charge contributions coming from water (solid blue line) and surfactant (solid red line). The specific water orientations and local dipoles of the surfactant conspire together to yield several layers of alternating positive and negative charges over a length scale of approximately 3 nm.

The origin of the modulated charge distribution at the water−C12E6 interface can be well understood by considering the separate contributions of the surfactant and the water molecules, as illustrated in Figure 5a. The interfacial charge distribution consists of two adjacent charge bilayers: (i) a major charge bilayer (Figure 5a,c, upper positive and negative layers) originating from the polarization between headgroups and hydrophobic tails and (ii) a minor (more subtle) charge bilayer (Figure 5a,c, lower positive and negative layers) arising from the interplay between water and headgroup relative orientations. The interfacial water molecules that are embedded by the hydrophobic tails have their OH groups directed toward the bulk, while the much more abundant hydrogen-bonded water molecules deeper down have their O−H groups pointing toward the interface, in particular toward the ether oxygen atoms of the surfactant headgroup. The net result of this charge distribution is a clear charge separation with the negative charge being located closer to the bulk in comparison to the positive charge. The molecular origins of these features are schematically summarized in the cartoon of Figure 5c.

The neat water−air interface features only a double layer of charge, as shown in Figure 5d. The upper positive charge is due to the dangling hydrogens from the disrupted hydrogen-bond network right at the interface. The oxygen atoms of these water molecules give rise to an excess negative charge that is closer to the bulk. The hydrogen-bonded water molecules have a net orientation that opposes this charge distribution, but this constitutes only a minor contribution.

As a consequence of the charge density distributions described above, an electrostatic potential arises across the interface. We determined the net total electric field, as well as the individual water and surfactant contributions (Figure 5b). The water−C12E6 interface is characterized by an electric field

https://doi.org/10.1021/jacs.1c05112
J. Am. Chem. Soc. XXXX, XXX, XXX−XXX

of ∼1 V/nm. Interestingly, the electric field at the air−water interface shown in Figure 5e has a similar magnitude but extends over a much shorter length scale of less than 0.5 nm.

While the values of electric fields at the water−surfactant and air−water interfaces are similar, the origins of the electric fields in the two systems are very different. The change in the sign of $\mathrm{Im}\chi^{(2)}$ in Figure 2b thus does not directly report on the magnitude of the total surface electric field but on the contribution of the hydrogen-bonded water molecules to this field. For the water−surfactant system this contribution dominates, while for neat water−air the surface electric field is dominated by the dangling OH groups (see Figure 5c,f).

It is important to note that local electric fields on the same order of magnitude as that mentioned above also exist around bulk water.[31] However, Figure 5 shows that, while the net electric field of bulk water is zero because of the randomized local orientation induced by thermal fluctuations, the interfacial arrangement of both water and surfactant creates a permanent nonzero electric field.

The surface potential measured by Kelvin-probe experiments can be directly compared with the electric potential, V_{MD}, determined from molecular dynamics simulations by integrating the electric field reported in Figure 4. The electric potentials obtained from the MD simulations are $V_{\mathrm{MD}}^{\mathrm{wat\text{-}surf}}$ = 1.15 V and $V_{\mathrm{MD}}^{\mathrm{wat\text{-}air}}$ = 0.62 V for the water−surfactant and water−air interfaces, respectively. Therefore, we can estimate the surface potential with the MD simulation values, yielding $V_{\mathrm{surf\,MD}} = V_{\mathrm{MD}}^{\mathrm{wat\text{-}surf}} - V_{\mathrm{MD}}^{\mathrm{wat\text{-}air}}$ = 0.53 V, which is in good agreement with the Kelvin-probe measurements (0.7 V). The consistency between the simulated and experimental measurements serves not only as a confirmation for the determined interfacial dielectric properties but also as a cross-validation for the numerical techniques employed, as well as the approximations involved in our calculations. It is clear that, in order to compute properties such as the SFG spectra, the inclusion of electronic polarization and charge transfer will be important, as has been shown in several studies.

PERSPECTIVES AND CONCLUSIONS

In this work, we have combined sum-frequency generation vibrational spectroscopy, Kelvin-probe surface potential measurements, and molecular dynamics simulations to study the structural and dielectric properties of the C12E6-surfactant interface. This surfactant is currently being prototyped for use in soap bubbles in applications for artificial photosynthesis (https://cordis.europa.eu/project/id/828838; https://sofiaproject.eu/).

We find that, close to the CMC, this nonionic surfactant creates an enhanced dynamically correlated hydrogen-bonding network, involving both penetrated water and surfactant groups. The surfactant also induces changes in the water orientations at the interface. These structural and orientational changes observed in the SFG are fully consistent with our MD simulations.

Surface potentials and electric fields have been discussed in both experimental and simulation contexts of various interfaces.[17,32] Very recently, there has been a growing interest in the use of electric fields to enhance catalytic processes in different types of chemical reactions.[3b,f,33] At the C12E6−water interface, we show that the structured hydrogen-bond network creates a region on the nanometer length scale with a net electric field on the order of 1 V/nm pointing from the vacuum to the bulk. These predictions from the simulations are subsequently confirmed by comparing with surface potential Kelvin-probe experiments. Even though the magnitudes of the fields are similar at the water−air and water−C12E6−air interfaces, the changes occur over different length scales (0.5 nm vs 3 nm), leading to a large difference in the magnitude of the surface potential.

One of the commonly employed models to interpret the surface potential from Kelvin-probe experiments considers a dipole field created by the surfactant molecules that is embedded in a continuum dielectric of solvent medium.[34] This model indicates that the interfacial water within the surfactant has a much smaller dielectric constant in comparison to bulk water. Similar features have been observed for water under confinement.[35] The reduction of the dielectric constant of water at the interface and the electric fields in this system arising from both the water and the surfactant molecules have enormous implications for their use in applications such as artificial photosynthesis and catalysis in general. More specifically, a photocatalytic molecule embedded in the surfactant will experience electric fields of varying magnitudes and directions depending on the extent of water or surfactant that surrounds it. Preliminary work from our group shows that electric fields like those observed in the C12E6−water system can change the HOMO−LUMO gap in ruthenium-based photocatalysts by at least 0.5 eV. Furthermore, it has been shown that water interfaces can exhibit much more chemical reactivity toward several volatile organic compounds.[36] These effects are expected to play a key role in chemical reactions associated with CO_2 reduction and water oxidation in artificial photosynthesis applications.

ASSOCIATED CONTENT

Supporting Information

The Supporting Information is available free of charge at https://pubs.acs.org/doi/10.1021/jacs.1c05112.

Additional experimental data from HD-VSFG experiments for different concentrations of C12E6, Kelvin-probe experiments done near the CMC for C12E6, and details of the Kelvin-probe experimental setup (PDF)

AUTHOR INFORMATION

Corresponding Authors

Huib J. Bakker − *AMOLF, 1098 XG Amsterdam, The Netherlands;* orcid.org/0000-0003-1564-5314; Email: H.Bakker@amolf.nl

Ali A. Hassanali − *International Centre for Theoretical Physics, 34151 Trieste, Italy;* orcid.org/0000-0002-3208-1488; Email: ahassana@ictp.it

Authors

Rahul Gera − *AMOLF, 1098 XG Amsterdam, The Netherlands;* orcid.org/0000-0001-6676-5768

Ricardo Franklin-Mergarejo − *International Centre for Theoretical Physics, 34151 Trieste, Italy*

Uriel N. Morzan − *International Centre for Theoretical Physics, 34151 Trieste, Italy*

Gabriele Falciani − *Energy Department, Politecnico di Torino, Torino 10129, Italy*

Luca Bergamasco − *Energy Department, Politecnico di Torino, Torino 10129, Italy*

Jan Versluis − *AMOLF, 1098 XG Amsterdam, The Netherlands*

https://doi.org/10.1021/jacs.1c05112
J. Am. Chem. Soc. XXXX, XXX, XXX−XXX

Indraneel Sen − *Uppsala University, 751 20 Uppsala, Sweden*
Silvia Dante − *Materials Characterization Facility, Italian Institute of Technology, 16163 Genoa, Italy;* orcid.org/0000-0001-6906-8482
Eliodoro Chiavazzo − *Energy Department, Politecnico di Torino, Torino 10129, Italy*

Complete contact information is available at: https://pubs.acs.org/10.1021/jacs.1c05112

Funding

This work has been funded by the European Commission in the framework of the project SoFiA − Soap Film based Artificial Photosynthesis−grant agreement 828838.

Notes

The authors declare no competing financial interest.

■ ACKNOWLEDGMENTS

R.G. would like to acknowledge Carolyn Moll from AMOLF for her input while analysis of SFG data and help with the experimental setup.

■ ABBREVIATIONS

HD-VSFG, heterodyne-detected vibrational sum frequency generation; MD, molecular dynamics; C12E6, hexaethylene glycol monododecyl ether; CMC, critical micelle concentration

■ REFERENCES

(1) (a) Nihonyanagi, S.; Yamaguchi, S.; Tahara, T. Ultrafast Dynamics at Water Interfaces Studied by Vibrational Sum Frequency Generation Spectroscopy. *Chem. Rev.* **2017**, *117*, 10665. (b) Laage, D.; Elsaesser, T.; Hynes, J. T. Water Dynamics in the Hydration Shells of Biomolecules. *Chem. Rev.* **2017**, *117*, 10694. (c) Jubb, A. M.; Hua, W.; Allen, H. C. Environmental Chemistry at Vapor/Water Interfaces: Insights from Vibrational Sum Frequency Generation Spectroscopy. *Annu. Rev. Phys. Chem.* **2012**, *63*, 107. (d) Björneholm, O.; Hansen, M. H.; Hodgson, A.; Liu, L.-M.; Limmer, D. T.; Michaelides, A.; Pedevilla, P.; Rossmeisl, J.; Shen, H.; Tocci, G.; Tyrode, E.; Walz, M.-M.; Werner, J.; Bluhm, H. Water at Interfaces. *Chem. Rev.* **2016**, *116*, 7698. (e) Park, J. Y.; Baker, L. R.; Somorjai, G. A. Role of Hot Electrons and Metal−Oxide Interfaces in Surface Chemistry and Catalytic Reactions. *Chem. Rev.* **2015**, *115*, 2781. (f) Geiger, F. M. Second Harmonic Generation, Sum Frequency Generation, and $\chi(3)$: Dissecting Environmental Interfaces with a Nonlinear Optical Swiss Army Knife. *Annu. Rev. Phys. Chem.* **2009**, *60*, 61.

(2) (a) Johnson, C. M.; Baldelli, S. Vibrational Sum Frequency Spectroscopy Studies of the Influence of Solutes and Phospholipids at Vapor/Water Interfaces Relevant to Biological and Environmental Systems. *Chem. Rev.* **2014**, *114*, 8416. (b) Pettersson, L. G. M.; Henchman, R. H.; Nilsson, A. Water—The Most Anomalous Liquid. *Chem. Rev.* **2016**, *116*, 7459. (c) Bellissent-Funel, M.-C.; Hassanali, A.; Havenith, M.; Henchman, R.; Pohl, P.; Sterpone, F.; van der Spoel, D.; Xu, Y.; Garcia, A. E. Water Determines the Structure and Dynamics of Proteins. *Chem. Rev.* **2016**, *116*, 7673.

(3) (a) Aragonès, A. C.; Haworth, N. L.; Darwish, N.; Ciampi, S.; Bloomfield, N. J.; Wallace, G. G.; Diez-Perez, I.; Coote, M. L. Electrostatic catalysis of a Diels−Alder reaction. *Nature* **2016**, *531*, 88. (b) Shaik, S.; Danovich, D.; Joy, J.; Wang, Z.; Stuyver, T. Electric-Field Mediated Chemistry: Uncovering and Exploiting the Potential of (Oriented) Electric Fields to Exert Chemical Catalysis and Reaction Control. *J. Am. Chem. Soc.* **2020**, *142*, 12551. (c) Ge, A.; Videla, P. E.; Lee, G. L.; Rudshteyn, B.; Song, J.; Kubiak, C. P.; Batista, V. S.; Lian, T. Interfacial Structure and Electric Field Probed by in Situ Electrochemical Vibrational Stark Effect Spectroscopy and Computational Modeling. *J. Phys. Chem. C* **2017**, *121*, 18674. (d) Sarkar, S.; Maitra, A.; Banerjee, S.; Thoi, V. S.; Dawlaty, J. M. Electric Fields at Metal−Surfactant Interfaces: A Combined Vibrational Spectroscopy and Capacitance Study. *J. Phys. Chem. B* **2020**, *124*, 1311. (e) Gallo, A.; Farinha, A. S. F.; Dinis, M.; Emwas, A.-H.; Santana, A.; Nielsen, R. J.; Goddard, W. A.; Mishra, H. The chemical reactions in electrosprays of water do not always correspond to those at the pristine air−water interface. *Chemical Science* **2019**, *10*, 2566. (f) Ruiz-Lopez, M. F.; Francisco, J. S.; Martins-Costa, M. T. C.; Anglada, J. M. Molecular reactions at aqueous interfaces. *Nature Reviews Chemistry* **2020**, *4*, 459. (g) Chen, L.; Feng, X. Enhanced catalytic reaction at an air−liquid−solid triphase interface. *Chemical Science* **2020**, *11*, 3124. (h) Barroo, C.; Wang, Z.-J.; Schlögl, R.; Willinger, M.-G. Imaging the dynamics of catalysed surface reactions by in situ scanning electron microscopy. *Nature Catalysis* **2020**, *3*, 30. (i) Ishizuka, S.; Hama, T.; Enami, S. Acid-Catalyzed Oligomerization at the Air−Water Interface Modified by Competitive Adsorption of Surfactants. *J. Phys. Chem. C* **2019**, *123*, 21662. (j) Yan, Z.; Zhu, L.; Li, Y. C.; Wycisk, R. J.; Pintauro, P. N.; Hickner, M. A.; Mallouk, T. E. The balance of electric field and interfacial catalysis in promoting water dissociation in bipolar membranes. *Energy Environ. Sci.* **2018**, *11*, 2235.

(4) (a) Kreuzer, H. J. Physics and chemistry in high electric fields. *Surf. Interface Anal.* **2004**, *36*, 372. (b) Siebert, T.; Guchhait, B.; Liu, Y.; Fingerhut, B. P.; Elsaesser, T. Range, Magnitude, and Ultrafast Dynamics of Electric Fields at the Hydrated DNA Surface. *J. Phys. Chem. Lett.* **2016**, *7*, 3131. (c) Lei, Y. K.; Zhang, J.; Zhang, Z.; Gao, Y. Q. Dynamic Electric Field Complicates Chemical Reactions in Solutions. *J. Phys. Chem. Lett.* **2019**, *10*, 2991. (d) Huang, X.; Tang, C.; Li, J.; Chen, L.-C.; Zheng, J.; Zhang, P.; Le, J.; Li, R.; Li, X.; Liu, J.; Yang, Y.; Shi, J.; Chen, Z.; Bai, M.; Zhang, H.-L.; Xia, H.; Cheng, J.; Tian, Z.-Q.; Hong, W. Electric field−induced selective catalysis of single-molecule reaction. *Science Advances* **2019**, *5*, eaaw3072.

(5) Yan, E. C. Y.; Liu, Y.; Eisenthal, K. B. New Method for Determination of Surface Potential of Microscopic Particles by Second Harmonic Generation. *J. Phys. Chem. B* **1998**, *102*, 6331.

(6) (a) Ong, S.; Zhao, X.; Eisenthal, K. B. Polarization of water molecules at a charged interface: second harmonic studies of the silica/water interface. *Chem. Phys. Lett.* **1992**, *191*, 327. (b) Zhang, C.; Sprik, M. Electromechanics of the liquid water vapour interface. *Phys. Chem. Chem. Phys.* **2020**, *22*, 10676.

(7) (a) Welborn, V. V.; Ruiz Pestana, L.; Head-Gordon, T. Computational optimization of electric fields for better catalysis design. *Nature Catalysis* **2018**, *1*, 649. (b) Welborn, V. V.; Li, W.-L.; Head-Gordon, T. Interplay of water and a supramolecular capsule for catalysis of reductive elimination reaction from gold. *Nat. Commun.* **2020**, *11*, 415.

(8) (a) Goates, S. R.; Schofield, D. A.; Bain, C. D. A Study of Nonionic Surfactants at the Air−Water Interface by Sum-Frequency Spectroscopy and Ellipsometry. *Langmuir* **1999**, *15*, 1400. (b) Mafi, A.; Hu, D.; Chou, K. C. Interactions of water with the nonionic surfactant polyoxyethylene glycol alkyl ethers studied by phase-sensitive sum frequency generation and molecular dynamics simulation. *Surf. Sci.* **2016**, *648*, 366. (c) Shang, B. Z.; Wang, Z.; Larson, R. G. Effect of Headgroup Size, Charge, and Solvent Structure on Polymer−Micelle Interactions, Studied by Molecular Dynamics Simulations. *J. Phys. Chem. B* **2009**, *113*, 15170. (d) Lu, J. R.; Thomas, R. K.; Penfold, J. Surfactant layers at the air/water interface: structure and composition. *Adv. Colloid Interface Sci.* **2000**, *84*, 143. (e) Lu, J. R.; Su, T. J.; Li, Z. X.; Thomas, R. K.; Staples, E. J.; Tucker, I.; Penfold, J. Structure of Monolayers of Monododecyl Dodecaethylene Glycol at the Air−Water Interface Studied by Neutron Reflection. *J. Phys. Chem. B* **1997**, *101*, 10332. (f) Lucassen-Reynders, E. H.; Cagna, A.; Lucassen, J. Gibbs elasticity, surface dilational modulus and diffusional relaxation in nonionic surfactant monolayers. *Colloids Surf., A* **2001**, *186*, 63. (g) Tyrode, E.; Johnson, C. M.; Rutland, M. W.; Claesson, P. M. Structure and Hydration of Poly(ethylene oxide) Surfactants at the Air/Liquid Interface. A Vibrational Sum Frequency Spectroscopy Study. *J. Phys. Chem. C* **2007**, *111*, 11642. (h) Falciani, G.; Franklin, R.; Cagna, A.; Sen, I.; Hassanali, A.; Chiavazzo, E. A multi-scale perspective of gas transport through soap-film membranes.

Molecular Systems Design & Engineering **2020**, *5*, 911. (i) Nikas, Y. J.; Puvvada, S.; Blankschtein, D. Surface tensions of aqueous nonionic surfactant mixtures. *Langmuir* **1992**, *8*, 2680. (j) Stubenrauch, C.; Claesson, P. M.; Rutland, M.; Manev, E.; Johansson, I.; Pedersen, J. S.; Langevin, D.; Blunk, D.; Bain, C. D. Mixtures of n-dodecyl-β-d-maltoside and hexaoxyethylene dodecyl ether — Surface properties, bulk properties, foam films, and foams. *Adv. Colloid Interface Sci.* **2010**, *155*, 5. (k) Shi, L.; Tummala, N. R.; Striolo, A. C12E6 and SDS Surfactants Simulated at the Vacuum−Water Interface. *Langmuir* **2010**, *26*, 5462.

(9) (a) Shen, Y. R. Phase-Sensitive Sum-Frequency Spectroscopy. *Annu. Rev. Phys. Chem.* **2013**, *64*, 129. (b) Eisenthal, K. B. Liquid interfaces. *Acc. Chem. Res.* **1993**, *26*, 636. (c) Bredenbeck, J.; Ghosh, A.; Nienhuys, H.-K.; Bonn, M. Interface-Specific Ultrafast Two-Dimensional Vibrational Spectroscopy. *Acc. Chem. Res.* **2009**, *42*, 1332. (d) Carter, J. A.; Wang, Z.; Dlott, D. D. Ultrafast Nonlinear Coherent Vibrational Sum-Frequency Spectroscopy Methods To Study Thermal Conductance of Molecules at Interfaces. *Acc. Chem. Res.* **2009**, *42*, 1343. (e) Ge, A.; Rudshteyn, B.; Videla, P. E.; Miller, C. J.; Kubiak, C. P.; Batista, V. S.; Lian, T. Heterogenized Molecular Catalysts: Vibrational Sum-Frequency Spectroscopic, Electrochemical, and Theoretical Investigations. *Acc. Chem. Res.* **2019**, *52*, 1289. (f) Shah, S. A.; Baldelli, S. Chemical Imaging of Surfaces with Sum Frequency Generation Vibrational Spectroscopy. *Acc. Chem. Res.* **2020**, *53*, 1139. (g) Wang, H.-F.; Gan, W.; Lu, R.; Rao, Y.; Wu, B.-H. Quantitative spectral and orientational analysis in surface sum frequency generation vibrational spectroscopy (SFG-VS). *Int. Rev. Phys. Chem.* **2005**, *24*, 191. (h) Wang, H.-F.; Velarde, L.; Gan, W.; Fu, L. Quantitative Sum-Frequency Generation Vibrational Spectroscopy of Molecular Surfaces and Interfaces: Lineshape, Polarization, and Orientation. *Annu. Rev. Phys. Chem.* **2015**, *66*, 189.

(10) Stiopkin, I. V.; Jayathilake, H. D.; Bordenyuk, A. N.; Benderskii, A. V. Heterodyne-Detected Vibrational Sum Frequency Generation Spectroscopy. *J. Am. Chem. Soc.* **2008**, *130*, 2271.

(11) (a) Strazdaite, S.; Versluis, J.; Backus, E. H. G.; Bakker, H. J. Enhanced ordering of water at hydrophobic surfaces. *J. Chem. Phys.* **2014**, *140*, 054711. (b) Strazdaite, S.; Versluis, J.; Bakker, H. J. Water orientation at hydrophobic interfaces. *J. Chem. Phys.* **2015**, *143*, 084708.

(12) (a) Nihonyanagi, S.; Ishiyama, T.; Lee, T.-k.; Yamaguchi, S.; Bonn, M.; Morita, A.; Tahara, T. Unified Molecular View of the Air/Water Interface Based on Experimental and Theoretical $\chi(2)$ Spectra of an Isotopically Diluted Water Surface. *J. Am. Chem. Soc.* **2011**, *133*, 16875. (b) Nihonyanagi, S.; Kusaka, R.; Inoue, K.-i.; Adhikari, A.; Yamaguchi, S.; Tahara, T. Accurate determination of complex $\chi(2)$ spectrum of the air/water interface. *J. Chem. Phys.* **2015**, *143*, 124707.

(13) Lu, J. R.; Li, Z. X.; Thomas, R. K.; Staples, E. J.; Tucker, I.; Penfold, J. Neutron reflection from a layer of monododecyl hexaethylene glycol adsorbed at the air-liquid interface: the configuration of the ethylene glycol chain. *J. Phys. Chem.* **1993**, *97*, 8012.

(14) Abraham, M. J.; Murtola, T.; Schulz, R.; Páll, S.; Smith, J. C.; Hess, B.; Lindahl, E. GROMACS: High performance molecular simulations through multi-level parallelism from laptops to supercomputers. *SoftwareX* **2015**, *1−2*, 19.

(15) Berendsen, H. J. C.; Postma, J. P. M.; van Gunsteren, W. F.; Hermans, J. In *Intermolecular Forces: Proceedings of the Fourteenth Jerusalem Symposium on Quantum Chemistry and Biochemistry Held in Jerusalem, Israel*, April 13−16, 1981; Pullman, B., Ed.; Springer Netherlands: 1981; p 331.

(16) (a) Jorgensen, W. L.; Maxwell, D. S.; Tirado-Rives, J. Development and Testing of the OPLS All-Atom Force Field on Conformational Energetics and Properties of Organic Liquids. *J. Am. Chem. Soc.* **1996**, *118*, 11225. (b) Siu, S. W. I.; Pluhackova, K.; Böckmann, R. A. Optimization of the OPLS-AA Force Field for Long Hydrocarbons. *J. Chem. Theory Comput.* **2012**, *8*, 1459. (c) Abdel-Azeim, S. Revisiting OPLS-AA Force Field for the Simulation of Anionic Surfactants in Concentrated Electrolyte Solutions. *J. Chem. Theory Comput.* **2020**, *16*, 1136.

(17) Zhang, H.; Singer, S. J. Analysis of the Subcritical Carbon Dioxide−Water Interface. *J. Phys. Chem. A* **2011**, *115*, 6285.

(18) Zhang, H.; Yin, C.; Jiang, Y.; van der Spoel, D. Force Field Benchmark of Amino Acids: I. Hydration and Diffusion in Different Water Models. *J. Chem. Inf. Model.* **2018**, *58*, 1037.

(19) Darden, T.; York, D.; Pedersen, L. Particle mesh Ewald: An N·log(N) method for Ewald sums in large systems. *J. Chem. Phys.* **1993**, *98*, 10089.

(20) Hess, B.; Bekker, H.; Berendsen, H. J. C.; Fraaije, J. G. E. M. LINCS: A linear constraint solver for molecular simulations. *J. Comput. Chem.* **1997**, *18*, 1463.

(21) Evans, D. J.; Holian, B. L. The Nose−Hoover thermostat. *J. Chem. Phys.* **1985**, *83*, 4069.

(22) (a) Giberti, F.; Hassanali, A. A. The excess proton at the air-water interface: The role of instantaneous liquid interfaces. *J. Chem. Phys.* **2017**, *146*, 244703. (b) Gasparotto, P.; Hassanali, A. A.; Ceriotti, M. Probing Defects and Correlations in the Hydrogen-Bond Network of ab Initio Water. *J. Chem. Theory Comput.* **2016**, *12*, 1953.

(23) Luzar, A.; Chandler, D. Hydrogen-bond kinetics in liquid water. *Nature* **1996**, *379*, 55.

(24) (a) Reiss, K.; Morzan, U. N.; Grigas, A. T.; Batista, V. S. Water Network Dynamics Next to the Oxygen-Evolving Complex of Photosystem II. *Inorganics* **2019**, *7*, 39. (b) Negre, C. F. A.; Morzan, U. N.; Hendrickson, H. P.; Pal, R.; Lisi, G. P.; Loria, J. P.; Rivalta, I.; Ho, J.; Batista, V. S. Eigenvector centrality for characterization of protein allosteric pathways. *Proc. Natl. Acad. Sci. U. S. A.* **2018**, *115*, E12201. (c) Newman, M. E. J. Modularity and community structure in networks. *Proc. Natl. Acad. Sci. U. S. A.* **2006**, *103*, 8577.

(25) Lange, O. F.; Grubmüller, H. Generalized correlation for biomolecular dynamics. *Proteins: Struct., Funct., Genet.* **2006**, *62*, 1053.

(26) Wijaya, E. C.; Separovic, F.; Drummond, C. J.; Greaves, T. L. Micelle formation of a non-ionic surfactant in non-aqueous molecular solvents and protic ionic liquids (PILs). *Phys. Chem. Chem. Phys.* **2016**, *18*, 24377.

(27) Tyrode, E.; Johnson, C. M.; Kumpulainen, A.; Rutland, M. W.; Claesson, P. M. Hydration State of Nonionic Surfactant Monolayers at the Liquid/Vapor Interface: Structure Determination by Vibrational Sum Frequency Spectroscopy. *J. Am. Chem. Soc.* **2005**, *127*, 16848.

(28) Butt, H. J.; Graf, K.; Kappl, M. *Physics and Chemistry of Interfaces*; Wiley: 2013.

(29) Nakahara, H.; Shibata, O.; Rusdi, M.; Moroi, Y. Examination of Surface Adsorption of Soluble Surfactants by Surface Potential Measurement at the Air/Solution Interface. *J. Phys. Chem. C* **2008**, *112*, 6398.

(30) Gonella, G.; Lütgebaucks, C.; de Beer, A. G. F.; Roke, S. Second Harmonic and Sum-Frequency Generation from Aqueous Interfaces Is Modulated by Interference. *J. Phys. Chem. C* **2016**, *120*, 9165.

(31) (a) Chalmet, S.; Ruiz-López, M. F. The reaction field of a water molecule in liquid water: Comparison of different quantum/classical models. *J. Chem. Phys.* **2001**, *115*, 5220. (b) Smith, J. D.; Cappa, C. D.; Wilson, K. R.; Cohen, R. C.; Geissler, P. L.; Saykally, R. J. Unified description of temperature-dependent hydrogen-bond rearrangements in liquid water. *Proc. Natl. Acad. Sci. U. S. A.* **2005**, *102*, 14171.

(32) (a) García Rey, N.; Weißenborn, E.; Schulze-Zachau, F.; Gochev, G.; Braunschweig, B. Quantifying Double-Layer Potentials at Liquid−Gas Interfaces from Vibrational Sum-Frequency Generation. *J. Phys. Chem. C* **2019**, *123*, 1279. (b) Dreier, L. B.; Nagata, Y.; Lutz, H.; Gonella, G.; Hunger, J.; Backus, E. H. G.; Bonn, M. Saturation of charge-induced water alignment at model membrane surfaces. *Science Advances* **2018**, *4*, eaap7415. (c) Jungwirth, P.; Tobias, D. J. Specific Ion Effects at the Air/Water Interface. *Chem. Rev.* **2006**, *106*, 1259.

(33) Che, F.; Gray, J. T.; Ha, S.; Kruse, N.; Scott, S. L.; McEwen, J.-S. Elucidating the Roles of Electric Fields in Catalysis: A Perspective. *ACS Catal.* **2018**, *8*, 5153.

(34) (a) Nakahara, H.; Shibata, O.; Moroi, Y. Examination of Surface Adsorption of Cetyltrimethylammonium Bromide and

https://doi.org/10.1021/jacs.1c05112
J. Am. Chem. Soc. XXXX, XXX, XXX−XXX

Sodium Dodecyl Sulfate. *J. Phys. Chem. B* **2011**, *115*, 9077. (b) Fernández Leyes, M.; Gimenez Reyes, S.; Cuenca, E.; Sánchez Morales, J. F.; Ritacco, H. Adsorption Kinetics of a Cationic Surfactant Bearing a Two-Charged Head at the Air-Water Interface. *Coatings* **2020**, *10*, 95.

(35) (a) Ahmadabadi, I.; Esfandiar, A.; Hassanali, A.; Ejtehadi, M. R. Structural and dynamical fingerprints of the anomalous dielectric properties of water under confinement. *Physical Review Materials* **2021**, *5*, 024008. (b) Schlaich, A.; Knapp, E. W.; Netz, R. R. Water Dielectric Effects in Planar Confinement. *Phys. Rev. Lett.* **2016**, *117*, 048001. (c) Zhu, H.; Yang, F.; Zhu, Y.; Li, A.; He, W.; Huang, J.; Li, G. Investigation of dielectric constants of water in a nano-confined pore. *RSC Adv.* **2020**, *10*, 8628. (d) Senapati, S.; Chandra, A. Dielectric Constant of Water Confined in a Nanocavity. *J. Phys. Chem. B* **2001**, *105*, 5106. (e) Fumagalli, L.; Esfandiar, A.; Fabregas, R.; Hu, S.; Ares, P.; Janardanan, A.; Yang, Q.; Radha, B.; Taniguchi, T.; Watanabe, K.; Gomila, G.; Novoselov, K. S.; Geim, A. K. Anomalously low dielectric constant of confined water. *Science* **2018**, *360*, 1339.

(36) (a) Kuo, I. F. W.; Mundy, C. J. An ab Initio Molecular Dynamics Study of the Aqueous Liquid-Vapor Interface. *Science* **2004**, *303*, 658. (b) Martins-Costa, M. T. C.; Anglada, J. M.; Francisco, J. S.; Ruiz-Lopez, M. F. Reactivity of Volatile Organic Compounds at the Surface of a Water Droplet. *J. Am. Chem. Soc.* **2012**, *134*, 11821. (c) Qiu, J.; Ishizuka, S.; Tonokura, K.; Colussi, A. J.; Enami, S. Reactivity of Monoterpene Criegee Intermediates at Gas−Liquid Interfaces. *J. Phys. Chem. A* **2018**, *122*, 7910.

https://doi.org/10.1021/jacs.1c05112
J. Am. Chem. Soc. XXXX, XXX, XXX−XXX